

Ordered Growth of Topological Insulator Bi₂Se₃ Thin Films on Dielectric Amorphous SiO₂ by MBE[†]

Sahng-Kyoon Jerng,^a Kisu Joo,^b Youngwook Kim,^c Sang-Moon Yoon,^d Jae Hong Lee,^a Miyoung Kim,^d Jun Sung Kim,^c Euijoon Yoon,^b Seung-Hyun Chun,^a and Yong Seung Kim^{a,*}

^a Department of Physics and Graphene Research Institute, Sejong University, Seoul 143-747, Korea

^b Department of Nano Science and Technology, Graduate School of Convergence Science and Technology, Seoul National University, Suwon 443-270, Korea

^c Department of Physics, Pohang University of Science and Technology, Pohang 790-784, Korea

^d Department of Materials Science and Engineering, Seoul National University, Seoul 151-744, Korea

[†]Electronic supplementary information (ESI) is available: Influence of Se passivation, RHEED patterns during the growth and annealing procedures, RHEED pattern and XRD profile of epitaxially grown Bi₂Se₃ films on Al₂O₃(0001) substrate, additional HRTEM images, AFM images, and Hall effect measurements.

* Corresponding Author: FAX: +82 2 3408 4316. E-mail address: yongskim77@gmail.com (Y. S. Kim)

Abstract

Topological insulators (TIs) are exotic materials which have topologically protected states on the surface due to the strong spin-orbit coupling. However, a lack of ordered growth of TI thin films on amorphous dielectrics and/or insulators presents a challenge for applications of TI-junctions. We report the growth of topological insulator Bi_2Se_3 thin films on amorphous SiO_2 by molecular beam epitaxy (MBE). To achieve the ordered growth of Bi_2Se_3 on amorphous surface, the formation of other phases at the interface is suppressed by Se passivation. Structural characterizations reveal that Bi_2Se_3 films are grown along the [001] direction with a good periodicity by van der Waals epitaxy mechanism. Weak anti-localization effect of Bi_2Se_3 films grown on amorphous SiO_2 shows modulated electrical property by the gating response. Our approach for ordered growth of Bi_2Se_3 on amorphous dielectric surface presents considerable advantages for TI-junctions with amorphous insulator or dielectric thin films.

Introduction

Topological insulators (TIs) are recently emerging new class of materials which have topologically protected states on the surface.¹ Due to the strong spin-orbit coupling, the surface states exhibit distinct features such as Dirac linear energy dispersion inside the bulk gap, spin-polarization by spin-momentum locking nature, and weak anti-localization (WAL).¹⁻⁵ These physical phenomena have created immense interests in the past few years. Among chalcogenide compounds, Bi_2Se_3 has attracted a special attention as three-dimensional TIs because it has the largest bulk band gap of 0.3 eV and a well-defined single Dirac cone at the momentum zero point in k space.^{2, 5} So far, mechanical exfoliations from single crystals^{6, 7} have been widely used to obtain high quality Bi_2Se_3 on dielectric substrates, which show limited lateral sizes of only few micrometers with irregular shapes. However, for practical applications of TIs, the growth of large-scale TI thin films on dielectrics or insulators is a challenge to advance forward. For example, low-power spintronic applications could be facilitated by developing TI tunnel junctions with dielectric or ferromagnetic insulators.⁸ Also, multichannel Dirac fermions could be utilized in spintronics by inserting normal insulators between multiple TI layers.^{9, 10}

Since the widely used dielectrics or insulators (such as SiO_2 , HfO_2 , and Al_2O_3) for device applications are formed in amorphous states, the growth of Bi_2Se_3 thin films on amorphous surface is urgently needed for TI study, which can be appealing for both fundamental physics and device applications. Recently, vapor-solid synthesis method is utilized to grow few-layer nanoplates of Bi_2Se_3 on amorphous dielectric,¹¹ but the lateral sizes did not exceed several micrometers. On the other hand, molecular beam epitaxy (MBE) technique has an advantage to grow large-area Bi_2Se_3 thin films with controllability of thickness.^{12, 13} To date, however, only crystalline substrates (such as Si, GaAs, Al_2O_3 , etc.) have been used to grow Bi_2Se_3 films on them.¹²⁻²⁴ In this paper, we report an approach to grow large-scale Bi_2Se_3 thin films on

amorphous SiO₂ by MBE. As a substrate, we chose 300 nm thick amorphous SiO₂ on Si(100), which had been widely used for bottom-gating experiments of Bi₂Se₃ flakes.^{6, 7, 11} At the initial stage of epitaxial growth, the formation of crystalline Bi₂Se₃ was hindered by the dangling bonds of surface defects, which was observed by *in situ* reflection high-energy electron diffraction (RHEED). However, by applying Se passivation to the surface, we were able to grow c-axis oriented Bi₂Se₃ films on amorphous SiO₂ with the aid of strain relaxation by van der Waals epitaxy mechanism. Structural characterizations by high-resolution transmission electron microscopy (HRTEM) show a periodicity of Bi₂Se₃ film along the [001] direction. Even though Bi₂Se₃ films were grown on amorphous surface, electrical transport measurements show the typically observed WAL effects in TI films and can be further modulated via bottom-gating. This growth compatibility of Bi₂Se₃ and amorphous dielectrics will stimulate the fabrication of TI hetero-junctions for practical applications.

Experimental section

Growth

Bi₂Se₃ thin films were grown by a home-made MBE system which was equipped with Knudsen cells and high purity bismuth (99.999+%) and selenium (99.999%) sources. The working pressure was less than 2.0×10^{-9} Torr with liquid nitrogen flowing in the shroud. SiO₂ substrates, cleaned by acetone and isopropyl alcohol prior to Bi₂Se₃ growth, were heated up to 120 °C for 30 minutes by a tungsten filament behind the sample manipulator in ultrahigh vacuum chamber to remove residual contaminations. The passivation process of surface dangling bonds was conducted by exposing the SiO₂ substrate to Se flux at 120 °C (this temperature is low enough to prevent the formation of second phases such as SiSe₂ and the Se layer could be self-limited without forming thick Se layer at this temperature).¹⁴ The substrate temperature was increased to

250 °C for the growth of Bi₂Se₃ thin films. A quartz crystal microbalance thickness monitor (Inficon SQM160) was used to calibrate the ratio of Bi and Se fluxes. The deposition rate of Bi₂Se₃ films was ~0.67 Å/min in this study. The ratio of Bi and Se flux was kept at ~1:15 to minimize Se vacancies.^{12, 21, 25} The formation of crystalline Bi₂Se₃ on the substrate is monitored by *in situ* RHEED pattern. For electrical transport measurements, samples were capped by Se layers on top after Bi₂Se₃ growth in order to minimize the contamination and/or doping effect from air exposure.²⁶

Characterization

Raman spectroscopy measurement was carried out using a micro-Raman spectroscopy system (Renishaw inVia) with a 514.5 nm laser excitation source. The incident laser had a power of 3.75 μW and was focused through an 100x objective. The spectra were calibrated by the Si peak at 520 cm⁻¹. X-ray diffraction (XRD) patterns were obtained using a X-ray diffractometer (Bruker D8 Advance) with Cu Kα radiation of wavelength 1.5406 Å. Interface studies were carried out using a HRTEM (Tecnai F20) operated at 200 kV. TEM samples were prepared by standard mechanical polishing. Surface morphology of the samples was evaluated by a commercial atomic force microscopy (AFM, PSIA XEI100). Low-temperature transport properties were measured by using the standard six-probe method in physical property measurement system (PPMS, Quantum Design).

Results and discussion

The sequence of the layered Bi₂Se₃ is Se-Bi-Se-Bi-Se which called a quintuple layer (QL, corresponding to ~0.955 nm) as shown in Fig. 1a. The surface is terminated by Se atoms without dangling bonds, resulting in only weak van der Waals (vdW) forces between each QL. Due to a weak interaction of overlayer with the substrate, Bi₂Se₃ can be grown epitaxially even on highly

lattice mismatched surface, which is called van der Waals epitaxy (vdWE).^{27, 28} We tried to grow crystalline Bi₂Se₃ thin films on amorphous SiO₂ via vdWE, and found that the crystallinity of Bi₂Se₃ thin film could be further enhanced by Se passivation of surface dangling bonds on SiO₂ substrate. As shown in Fig. 1b, the RHEED pattern of SiO₂ is a haze due to the amorphous surface. When the Bi₂Se₃ film is grown on unpassivated SiO₂, the RHEED pattern changes to the spotty patterns (marked by white arrows in Fig. 1c) which indicate that the growth of Bi₂Se₃ is encumbered by a formation of other phases (see also the ESI). On the other hand, a streaky RHEED pattern of crystalline Bi₂Se₃ is observed when the growth proceeds on Se passivated SiO₂ surface (Fig. 1d), indicating enhanced crystallinity of Bi₂Se₃. Once the surface dangling bonds are saturated, chemical bond formation between the substrate and TI components can be prevented.¹⁴ Additionally, enlarged grain sizes of Bi₂Se₃ at the initial stage are observed on Se passivated SiO₂ (see AFM images in the ESI). Fig. 1e shows a photograph of Bi₂Se₃ film grown on 1.5 x 1.5 cm² substrate (edges of substrate were masked by a Mo holder).

To investigate the film crystallinity, as-grown 20 nm thick Bi₂Se₃ films on amorphous SiO₂ were identified by XRD. Fig. 2a shows that the XRD profile contains only the (003) family of diffraction peaks in the θ -2 θ scan, whose positions agree well with those of c-axis oriented epitaxial Bi₂Se₃ films (see the ESI) and bulk values.¹² Fig. 2b shows the vibrational modes and the Raman spectra in the range of 100—200 cm⁻¹. Within these frequencies, two characteristic peaks were observed at ~131 cm⁻¹ and ~174 cm⁻¹, which correspond to an in-plane mode (E_g²) and an out-of-plane mode (A_{1g}²) of rhombohedral Bi₂Se₃ lattice vibrations, respectively.^{16, 29-31}

For detailed structural information, the cross-sectional HRTEM was used to examine the microstructure of Bi₂Se₃ film grown on SiO₂ substrate. Fig. 3a and 3b show the HRTEM images of periodic atomic structure of Bi₂Se₃ on amorphous SiO₂ substrate. As marked by orange colored arrows in Fig. 3a, some structural faults are observed in Bi₂Se₃ film, which are similarly

observed in a recent study of MBE grown Bi_2Se_3 films on highly mismatched crystalline substrates.¹⁸ This result can be attributed to the slightly wavy surface of substrate and the surface roughness of substrate. Note that the difference of surface potentials, correlated with roughness such as point defects, affects the initial growth of Bi_2Se_3 films on amorphous substrate. As shown in Fig. 3b, initial 1—2 QLs (orange colored arrow) are not exactly parallel to the surface near the small puddle of SiO_2 surface. However, after the puddle is filled with initial few layers, the strain is released along the growth direction due to the vdWE mechanism. The HRTEM image of high magnification (Fig. 3b) clearly reveals the crystalline structure of Bi_2Se_3 along the [001] direction with the distance of 0.965 nm between QLs (white dot lines), which is consistent with the cross-sectional height (~ 0.96 nm) of triangular feature on the top surface (see AFM images in the ESI). These results show that our approach achieved the ordered growth of Bi_2Se_3 thin films on amorphous surface. Furthermore, we infer that other layered TI thin films of chalcogenide compounds can be grown on amorphous surface by using proper surface passivation technique such as *in situ* plasma treatment or exposure of chalcogen materials to saturate the dangling bonds.

Even though Bi_2Se_3 film was grown on amorphous surface, electrical transport measurements show typically observed WAL effects in TI films and can be further modulated via bottom-gating. As shown in the inset of Fig. 4a, the normalized magnetoresistance of 20 nm thick Bi_2Se_3 film shows a cusp at $B = 0$ T, which is a signature of WAL effect originated from quickly suppressed destructive quantum interferences between time-reversed paths in a perpendicular magnetic field.³² This WAL behavior reflects both the Dirac nature of the surface states and the strong spin-orbit interaction in the bulk of TIs.³³ The exact behavior of magnetoconductance $\Delta G(B)$ is described by the Hikami-Larkin-Nagaoka formula:³⁴ $\Delta G(B) = \alpha(e^2/\pi h)[\ln(B_\phi/B) - \Psi(1/2 + B_\phi/B)]$, where $\Delta G(B)$ is the low field magneto-conductance ($\Delta G(B) =$

$G(B)-G(0)$, B_ϕ is the dephasing magnetic field, Ψ is the digamma function, and α is a coefficient predicted to be 1/2 for each surface channel. Fig. 4a presents the magnetoconductance at various gate voltages (V_g); the gate contact was simply made to the bottom of p-type Si substrate using amorphous SiO_2 as dielectrics. The obtained value of α is close to 1/2 (~ 0.43 at $V_g = -50$ V), shown in upper panel of Fig. 4b, implying that the top and bottom surfaces are coupled through the bulk to form a single effective channel for the phase-coherent transport.^{10, 11, 35} Note that the coefficient α decreases from 0.43 to 0.39 (upper panel of Fig. 4b) while the carrier concentration increases from 3.4 to $4.8 \times 10^{13} \text{ cm}^{-2}$ (lower panel of Fig. 4b, extracted from the Hall measurements, see also the ESI) as the V_g increases from -50 to 50 V. This is probably due to the fact that the bulk carriers contribute more to the overall conductivity of the system with the increasing gate voltage.³⁵ Therefore, further improvements should be possible by reducing the bulk carrier concentration through Ca doping or gating with a high-k dielectric layer.^{6, 20, 33} The existence of the WAL effect with the gating response bears a considerable potential in the application of our approach for TI-junctions of Bi_2Se_3 films and dielectrics or insulators which are formed in amorphous states.

Conclusions

In conclusion, we demonstrate the ordered growth of Bi_2Se_3 thin films on the dielectric amorphous SiO_2 surface by vdWE. Passivation of the dangling bonds was accomplished by low-temperature Se exposure. Structural characterizations show that c-axis oriented Bi_2Se_3 films were grown on SiO_2 surface via vdW coupling. Low-temperature transport measurements show the WAL effect and bottom-gating responses, which suggest that Bi_2Se_3 films directly grown on amorphous SiO_2 exhibit the surface state properties of TI materials. Our results will stimulate the application of TI materials in combination with amorphous dielectrics.

Acknowledgements

This research was supported by the Priority Research Centers Program (2012-0005859), the Basic Science Research Program (2012-0007298, 2012-040278, 2012-013838), the Center for Topological Matter in POSTECH (2012-0009194), and the Nanomaterial Technology Development Program (2012M3A7B4049888) through the National Research Foundation of Korea (NRF) funded by the Ministry of Education, Science and Technology (MEST).

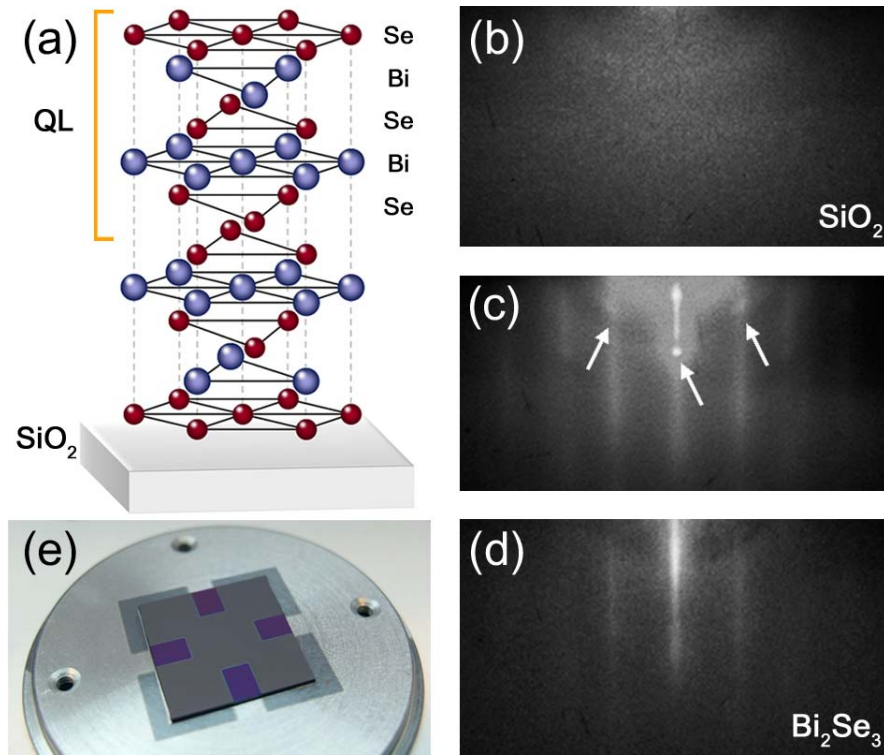


Fig. 1 (a) Schematic illustration of Bi₂Se₃ structure on SiO₂ substrate. RHEED patterns of (b) amorphous SiO₂ substrate, (c) other phase of Bi₂Se₃ grown on unpassivated SiO₂, and (d) crystalline Bi₂Se₃ grown on Se passivated SiO₂. (e) Photograph of Bi₂Se₃/SiO₂ specimen (1.5 cm x 1.5 cm).

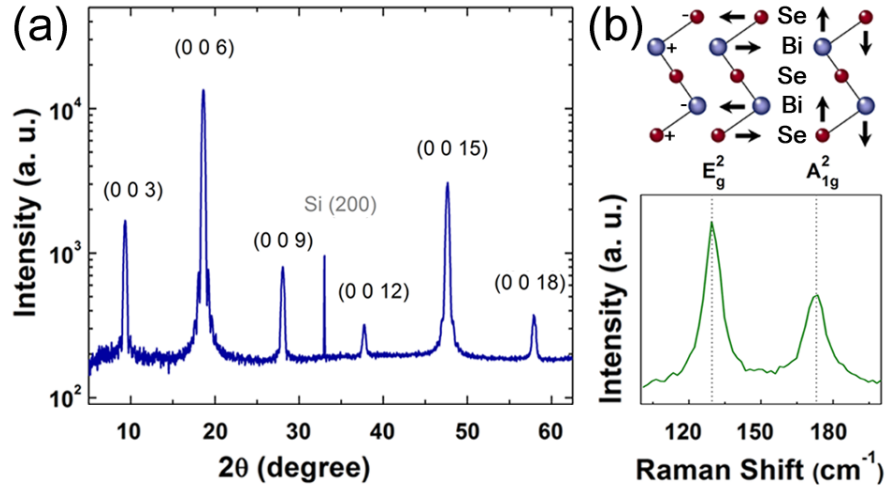


Fig. 2 The structural characterizations of 20 nm thick Bi_2Se_3 thin films. (a) XRD pattern in the θ - 2θ scan. (b) Schematic of vibrational modes and corresponding Raman spectra.

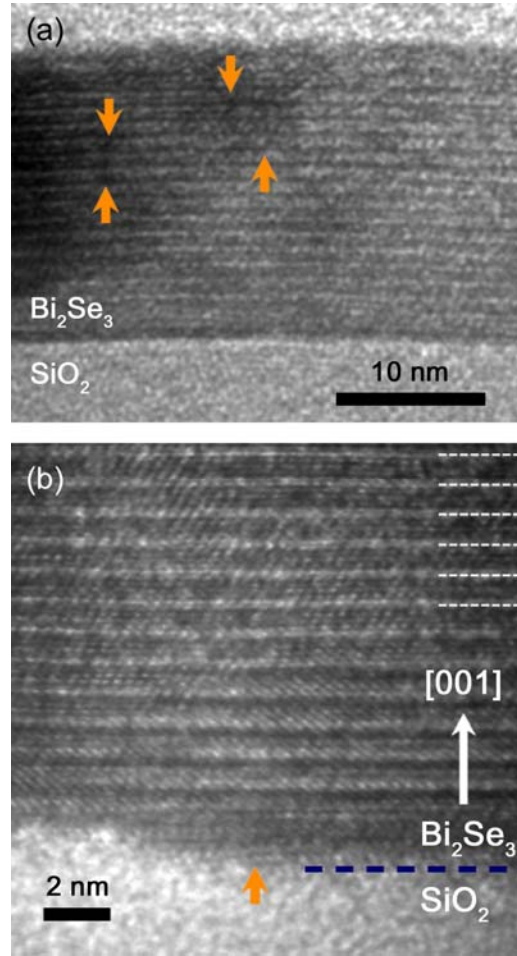


Fig. 3 Cross-sectional HRTEM images at (a) low magnification and (b) high magnification. Some structural faults are observed within Bi_2Se_3 and at the interface with SiO_2 (pointed by the orange colored arrows). The dotted lines indicate QLs.

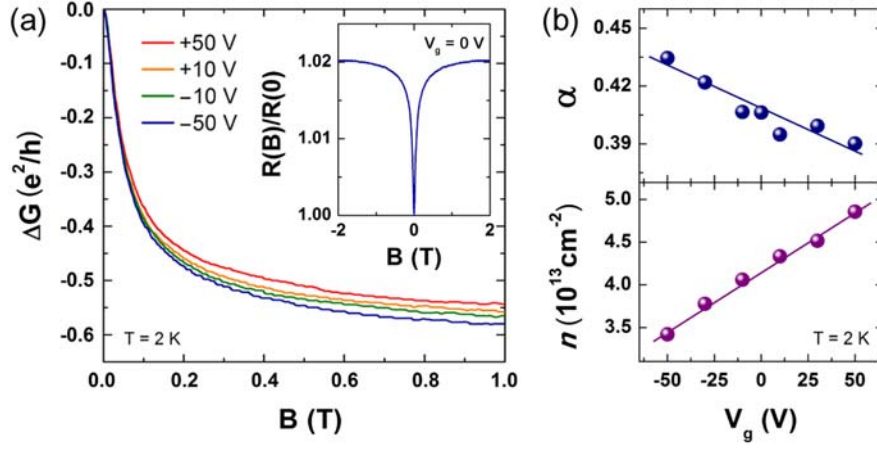


Fig. 4 Electrical transport measurements of a 20 nm thick Bi_2Se_3 film at 2 K. (a) Gate voltage dependence of the WAL effect and (inset) normalized magnetoresistance at zero gate voltage. (b) The fitting coefficient α from Hikami-Larkin-Nagaoka theory (upper panel) and gate voltage dependence of the areal carrier concentration (lower panel).

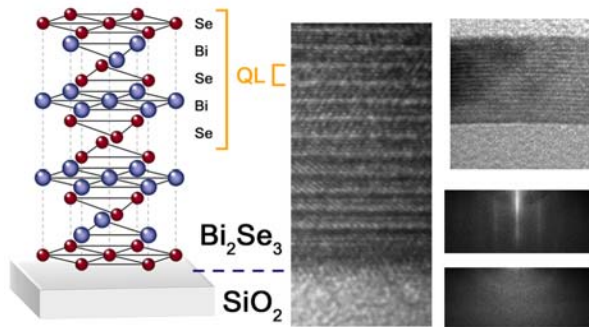
References

1. H. J. Zhang, C. X. Liu, X. L. Qi, X. Dai, Z. Fang and S. C. Zhang, *Nat Phys*, 2009, **5**, 438-442.
2. D. Hsieh, Y. Xia, D. Qian, L. Wray, J. H. Dil, F. Meier, J. Osterwalder, L. Patthey, J. G. Checkelsky, N. P. Ong, A. V. Fedorov, H. Lin, A. Bansil, D. Grauer, Y. S. Hor, R. J. Cava and M. Z. Hasan, *Nature*, 2009, **460**, 1101-1106.
3. L. Fu, C. L. Kane and E. J. Mele, *Phys Rev Lett*, 2007, **98**, 106803.
4. H. T. He, G. Wang, T. Zhang, I. K. Sou, G. K. L. Wong, J. N. Wang, H. Z. Lu, S. Q. Shen and F. C. Zhang, *Phys Rev Lett*, 2011, **106**, 166805.
5. Y. Xia, D. Qian, D. Hsieh, L. Wray, A. Pal, H. Lin, A. Bansil, D. Grauer, Y. S. Hor, R. J. Cava and M. Z. Hasan, *Nat Phys*, 2009, **5**, 398-402.
6. J. G. Checkelsky, Y. S. Hor, R. J. Cava and N. P. Ong, *Phys Rev Lett*, 2011, **106**, 196801.
7. H. Steinberg, D. R. Gardner, Y. S. Lee and P. Jarillo-Herrero, *Nano Lett*, 2010, **10**, 5032-5036.
8. B. D. Kong, Y. G. Semenov, C. M. Krowne and K. W. Kim, *Appl Phys Lett*, 2011, **98**, 243112-3.
9. J. H. Song, H. Jin and A. J. Freeman, *Phys Rev Lett*, 2010, **105**, 096403.
10. Z. Y. Wang, X. Guo, H. D. Li, T. L. Wong, N. Wang and M. H. Xie, *Appl Phys Lett*, 2011, **99**, 023112.
11. D. S. Kong, W. H. Dang, J. J. Cha, H. Li, S. Meister, H. L. Peng, Z. F. Liu and Y. Cui, *Nano Lett*, 2010, **10**, 2245-2250.
12. Y. S. Kim, M. Brahlek, N. Bansal, E. Edrey, G. A. Kapilevich, K. Iida, M. Tanimura, Y. Horibe, S. W. Cheong and S. Oh, *Phys Rev B*, 2011, **84**, 073109.
13. A. A. Taskin, S. Sasaki, K. Segawa and Y. Ando, *Phys Rev Lett*, 2012, **109**, 066803.

14. N. Bansal, Y. S. Kim, E. Edrey, M. Brahlek, Y. Horibe, K. Iida, M. Tanimura, G. H. Li, T. Feng, H. D. Lee, T. Gustafsson, E. Andrei and S. Oh, *Thin Solid Films*, 2011, **520**, 224-229.
15. G. H. Zhang, H. J. Qin, J. Teng, J. D. Guo, Q. L. Guo, X. Dai, Z. Fang and K. H. Wu, *Appl Phys Lett*, 2009, **95**, 053114.
16. X. Liu, D. J. Smith, J. Fan, Y. H. Zhang, H. Cao, Y. P. Chen, J. Leiner, B. J. Kirby, M. Dobrowolska and J. K. Furdyna, *Appl Phys Lett*, 2011, **99**, 171903.
17. A. Richardella, D. M. Zhang, J. S. Lee, A. Koser, D. W. Rench, A. L. Yeats, B. B. Buckley, D. D. Awschalom and N. Samarth, *Appl Phys Lett*, 2010, **97**, 262104.
18. N. V. Tarakina, S. Schreyeck, T. Borzenko, C. Schumacher, G. Karczewski, K. Brunner, C. Gould, H. Buhmann and L. W. Molenkamp, *Cryst Growth Des*, 2012, **12**, 1913-1918.
19. X. F. Kou, L. He, F. X. Xiu, M. R. Lang, Z. M. Liao, Y. Wang, A. V. Fedorov, X. X. Yu, J. S. Tang, G. Huang, X. W. Jiang, J. F. Zhu, J. Zou and K. L. Wang, *Appl Phys Lett*, 2011, **98**, 242102.
20. G. H. Zhang, H. J. Qin, J. Chen, X. Y. He, L. Lu, Y. Q. Li and K. H. Wu, *Adv Funct Mater*, 2011, **21**, 2351-2355.
21. P. Tabor, C. Keenan, S. Urazdhin and D. Lederman, *Appl Phys Lett*, 2011, **99**, 013111.
22. N. Bansal, Y. S. Kim, M. Brahlek, E. Edrey and S. Oh, *Phys Rev Lett*, 2012, **109**, 116804.
23. C. L. Song, Y. L. Wang, Y. P. Jiang, Y. Zhang, C. Z. Chang, L. L. Wang, K. He, X. Chen, J. F. Jia, Y. Y. Wang, Z. Fang, X. Dai, X. C. Xie, X. L. Qi, S. C. Zhang, Q. K. Xue and X. C. Ma, *Appl Phys Lett*, 2010, **97**, 143118.
24. Z. Y. Wang, H. D. Li, X. Guo, W. K. Ho and M. H. Xie, *J Cryst Growth*, 2011, **334**, 96-102.
25. H. Okamoto, *JPE*, 1994, **15**, 195-201.

26. M. H. Liu, C. Z. Chang, Z. C. Zhang, Y. Zhang, W. Ruan, K. He, L. L. Wang, X. Chen, J. F. Jia, S. C. Zhang, Q. K. Xue, X. C. Ma and Y. Y. Wang, *Phys Rev B*, 2011, **83**, 165440.
27. A. D. Novaco and J. P. McTague, *Phys Rev Lett*, 1977, **38**, 1286-1289.
28. A. Koma, *Thin Solid Films*, 1992, **216**, 72-76.
29. W. H. Dang, H. L. Peng, H. Li, P. Wang and Z. F. Liu, *Nano Lett*, 2010, **10**, 2870-2876.
30. J. Zhang, Z. P. Peng, A. Soni, Y. Y. Zhao, Y. Xiong, B. Peng, J. B. Wang, M. S. Dresselhaus and Q. H. Xiong, *Nano Lett*, 2011, **11**, 2407-2414.
31. K. M. F. Shahil, M. Z. Hossain, V. Goyal and A. A. Balandin, *J Appl Phys*, 2012, **111**, 054305.
32. G. Bergmann, *Solid State Commun*, 1982, **42**, 815-817.
33. H. Steinberg, J. B. Laloe, V. Fatemi, J. S. Moodera and P. Jarillo-Herrero, *Phys Rev B*, 2011, **84**, 233101.
34. S. Hikami, A. I. Larkin and Y. Nagaoka, *Prog Theor Phys*, 1980, **63**, 707-710.
35. M. R. Lang, L. He, F. X. Xiu, X. X. Yu, J. S. Tang, Y. Wang, X. F. Kou, W. J. Jiang, A. V. Fedorov and K. L. Wang, *Acs Nano*, 2012, **6**, 295-302.

TOC



Topological insulator Bi_2Se_3 thin films are grown directly on oxidized amorphous silicon (SiO_2) substrate by molecular beam epitaxy with van der Waals epitaxy method.

Supplementary Information

Ordered Growth of Topological Insulator Bi_2Se_3 Thin Films on Dielectric amorphous SiO_2 by MBE

Sahng-Kyoon Jerng, Yong Seung Kim, Kisu Joo, Youngwook Kim, Sang-Moon Yoon, Jae Hong

Lee, Miyoung Kim, Jun Sung Kim, Euijoon Yoon, and Seung-Hyun Chun

1. The influence of Se passivation

Fig. S1a and b show AFM images of Bi_2Se_3 films grown on unpassivated SiO_2 surface and Se passivated SiO_2 surface, respectively. Surface morphology is obtained by commercial AFM (NanoFocus Inc). Both of samples were not annealed after growth of 2 hours. The morphology of as-grown films without passivation is exhibited small grains (Fig. S1a) and RHEED pattern was indicated a formation of other phase as shown in inset of Fig. S1a (marked by white arrow). On the other hand, as-grown films on Se passivated SiO_2 presents forming of large grains (Fig. S1b) and RHEED pattern of well-crystallized Bi_2Se_3 (the inset of Fig. S1b). The surface roughness is 0.54 nm and 0.66 nm for Bi_2Se_3 films grown on the unpassivated surface and the passivated surface, respectively.

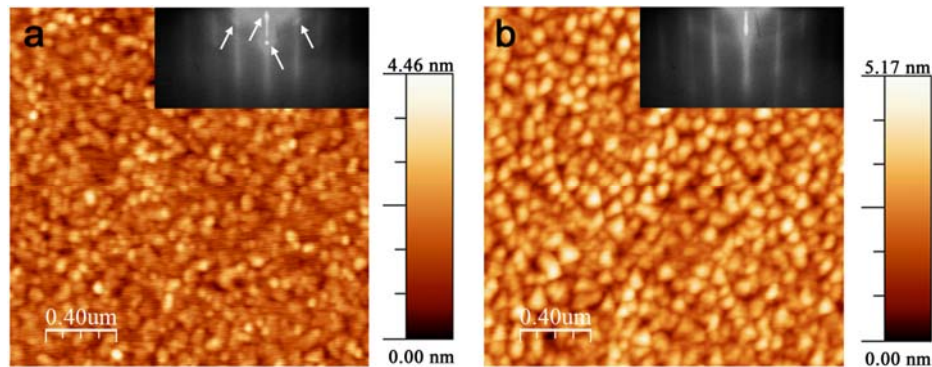


Fig. S1 AFM images of Bi₂Se₃ films for (a) grown on unpassivated SiO₂ surface and (b) Se passivated SiO₂ surface. The insets are RHEED patterns recorded during the growth.

2. RHEED patterns for Bi₂Se₃ growth procedures

Prior to the growth, samples were heated at 120 °C to remove residual contamination. Fig. S2a shows RHEED pattern of SiO₂ substrate at 120 °C, which is typical RHEED pattern for amorphous substrate. After 30 minutes, Se was deposited on SiO₂ surface. RHEED pattern was not changed from that of amorphous (Fig. S2b). Then, temperature increased to 250 °C for growth of Bi₂Se₃ films. During the growth, RHEED pattern is developed to streaky diffraction pattern as shown in Fig. S2c and S2d. After the growth, samples were annealed at 450 °C (Fig. S2e). RHEED patterns are not shown the formation of other phase in the annealing to cool down (Fig. S2f).

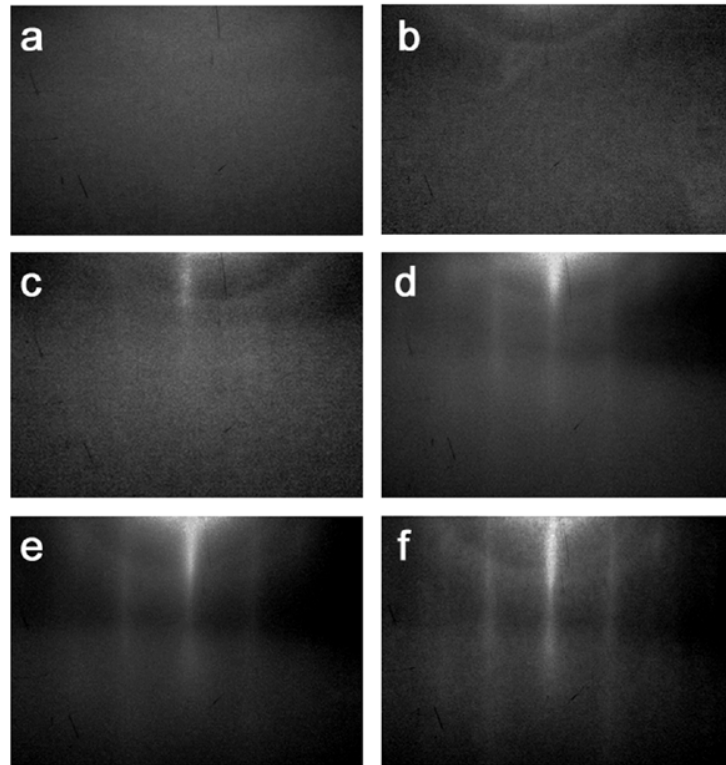


Fig. S2 RHEED patterns for Bi_2Se_3 growth procedures: (a) SiO_2 substrate at 120 °C, (b) Se exposure for passivation, (c)-(d) Bi_2Se_3 growth (RHEED recorded at 30 min and 90 min, respectively), (e) annealing at 450 °C for 30 min, and (f) cool down. The large dark features on the screen are shadows of the substrate holders.

3. RHEED pattern and XRD profile of epitaxially grown Bi_2Se_3 films on $\text{Al}_2\text{O}_3(0001)$ substrate

Fig. S3 provides RHEED patterns and XRD profile of MBE-grown epitaxial Bi_2Se_3 films on $\text{Al}_2\text{O}_3(0001)$, known as sapphire, substrate. As shown in Figure S3a, RHEED pattern indicates crystalline sapphire substrate. During the growth of Bi_2Se_3 at 250 °C, RHEED pattern changes to the crystalline Bi_2Se_3 . XRD profile, obtained by Shimadzu XRD-6100, reveals the (003) family of diffraction peak of c-axis oriented Bi_2Se_3 films as shown in Fig. S3c.

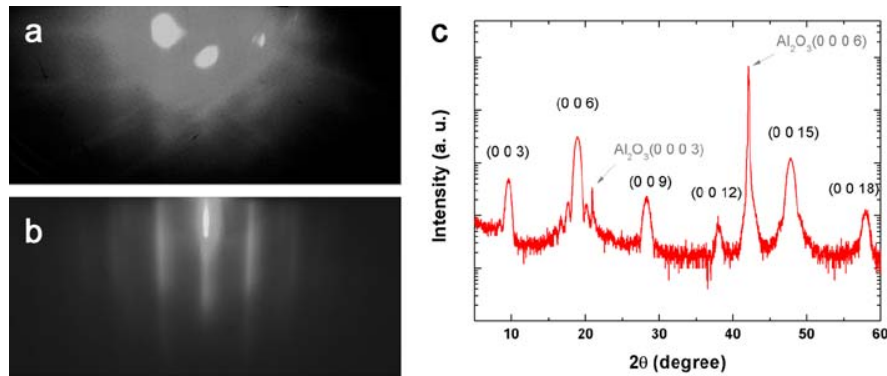


Fig. S3 RHEED pattern of (a) crystalline sapphire substrate and (b) epitaxially grown Bi_2Se_3 films. (c) XRD profile of MBE-grown Bi_2Se_3 films on sapphire substrate.

4. Additional HRTEM images of interface between Bi_2Se_3 films and flat SiO_2

Fig. S4 shows the HRTEM images for different Bi_2Se_3 thin film samples grown on SiO_2 . Additional HRTEM measurement was carried out using JEM-2100F instrument operated at 200 kV. Well-stacked Bi_2Se_3 quintuple layers are clearly observed.

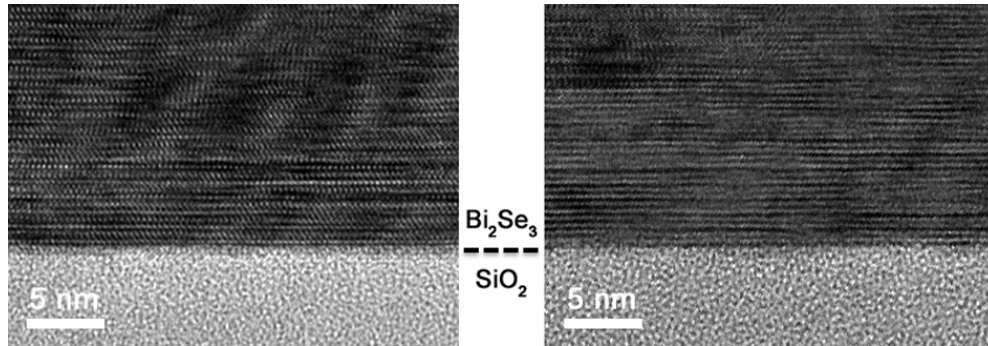


Fig. S4 HRTEM images for Bi_2Se_3 thin films grown on flat SiO_2 surface area.

5. Surface morphology of Bi_2Se_3 films grown on SiO_2

Fig. S5 shows the AFM image of a 20 nm thick Bi_2Se_3 thin film grown on SiO_2 . Terraces and/or steps (with triangular and hexagonal shapes) represent the 3-fold symmetry of Bi_2Se_3 . The cross-sectional height of triangular feature is ~ 0.96 nm. The disordered feature of triangular Bi_2Se_3 terraces along the in-plane directions can be attributed to the 300 nm thick amorphous SiO_2 surface which does not provide a lattice constraint for atom stacking during the deposition.

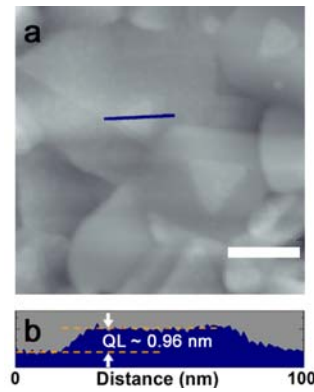


Fig. S5 (a) AFM image of a 20 nm thick film. Scale bar = 100 nm. (b) Cross-sectional profile along the line in (a) showing the QL of Bi₂Se₃.

6. Hall measurement for 20 nm thick films

Fig. S6 shows Hall resistance of 20 nm thick films in the perpendicular magnetic field. The standard six-probe method is used for Hall measurement ($I = 100 \mu\text{A}$, $T = 2 \text{ K}$). Sample is indicated as n-type semiconductor with a carrier concentration of $4.2 \times 10^{13} \text{ cm}^{-2}$ at $V_g = 0 \text{ V}$. The carrier density decreased down to $3.4 \times 10^{13} \text{ cm}^{-2}$ at $V_g = -50 \text{ V}$.

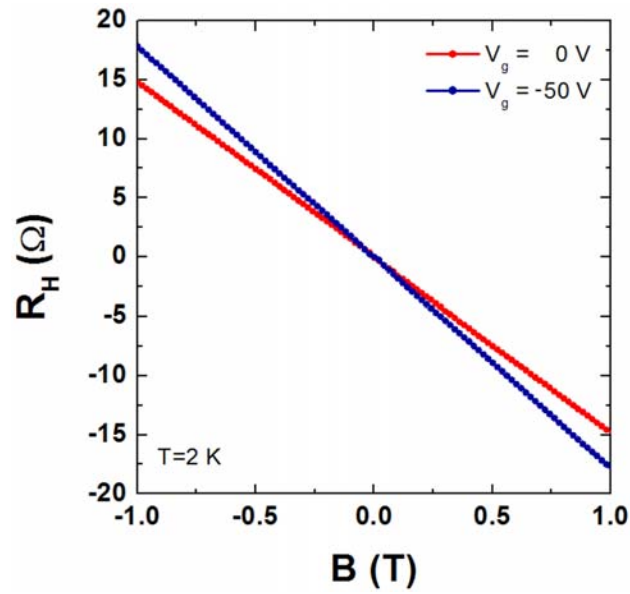


Fig. S6 Hall resistance of 20 nm thick films for applying gate voltage in the magnetic field of $\pm 1 \text{ T}$.